*pharmaceutics*

MDPI

*Article*

# New-Generation Heterocyclic Bis-Pentamethinium Salts as Potential Cytostatic Drugs with Dual IL-6R and Mitochondria-Targeting Activity

**Veronika Talianová [1,2], Zdeněk Kejík [1,2], Robert Kaplánek [1,2], Kateřina Veselá [1,2], Nikita Abramenko [1,2], Lukáš Lacina [1,3,4], Karolína Strnadová [1,3], Barbora Dvořánková [1,3], Pavel Martásek [2], Michal Masařík [1,2,5], Magdalena Houdová Megová [6], Petr Bušek [6,*], Jana Křížová [2], Lucie Zdražilová [2], Hana Hansíková [2], Erik Vlčák [7], Vlada Filimonenko [7], Aleksi Šedo [6], Karel Smetana, Jr. [1,3] and Milan Jakubek [1,2,*]**

1 BIOCEV, First Faculty of Medicine, Charles University, CZ-252 42 Vestec, Czech Republic
2 Department of Paediatrics and Inherited Metabolic Disorders, First Faculty of Medicine, Charles University and General University Hospital, Ke Karlovu 455/2, Prague 2, CZ-128 08 Prague, Czech Republic
3 Institute of Anatomy, First Faculty of Medicine, Charles University, Prague 2, CZ-120 00 Prague, Czech Republic
4 Department of Dermatovenerology, First Faculty of Medicine, Charles University and General University Hospital, CZ-128 08 Prague, Czech Republic
5 Department of Pathological Physiology and Department of Physiology, Faculty of Medicine, Masaryk University, Kamenice 5, CZ-625 00 Brno, Czech Republic
6 Institute of Biochemistry and Experimental Oncology, First Faculty of Medicine, Charles University, Prague 2, CZ-120 00 Prague, Czech Republic
7 Institute of Molecular Genetics, Academy of Sciences, Prague 4, CZ-140 00 Prague, Czech Republic
* Correspondence: petr.busek2@lf1.cuni.cz (P.B.); milan.jakubek@lf1.cuni.cz (M.J.)

check for updates

**Citation:** Talianová, V.; Kejík, Z.; Kaplánek, R.; Veselá, K.; Abramenko, N.; Lacina, L.; Strnadová, K.; Dvořánková, B.; Martásek, P.; Masařík, M.; et al. New-Generation Heterocyclic Bis-Pentamethinium Salts as Potential Cytostatic Drugs with Dual IL-6R and Mitochondria-Targeting Activity. *Pharmaceutics* **2022**, *14*, 1712. https://doi.org/10.3390/pharmaceutics14081712

Academic Editor: Murali Mohan Yallapu

Received: 4 July 2022
Accepted: 12 August 2022
Published: 17 August 2022

**Publisher's Note:** MDPI stays neutral with regard to jurisdictional claims in published maps and institutional affiliations.



**Abstract:** IL-6 signaling is involved in the pathogenesis of a number of serious diseases, including chronic inflammation and cancer. Targeting of IL-6 receptor (IL-6R) by small molecules is therefore an intensively studied strategy in cancer treatment. We describe the design, synthesis, and characteristics of two new bis-pentamethinium salts **5** and **6** (meta and para) bearing indole moieties. Molecular docking studies showed that both compounds have the potential to bind IL-6R (free energy of binding −9.5 and −8.1 kcal/mol). The interaction with IL-6R was confirmed using microscale thermophoresis analyses, which revealed that both compounds had strong affinity for the IL-6R (experimentally determined dissociation constants 26.5 ± 2.5 nM and 304 ± 27.6 nM, respectively). In addition, both compounds were cytotoxic for a broad spectrum of cancer cell lines in micromolar concentrations, most likely due to their accumulation in mitochondria and inhibition of mitochondrial respiration. In summary, the structure motif of bis-pentamethinium salts represents a promising starting point for the design of novel multitargeting compounds with the potential to inhibit IL-6 signaling and simultaneously target mitochondrial metabolism in cancer cells.

**Keywords:** IL-6R synthetic inhibitors; mitochondria; cancer

## 1. Introduction

Interleukin-6 (IL-6) is a multifunctional proinflammatory mediator that was originally identified as a T-cell-derived cytokine inducing terminal maturation in antibody-producing B cells [1]. It is known under different synonyms (interferon β2, 26 K factor, hybridoma growth factor, plasmocytoma growth factor, hepatocyte stimulatory factor, hematopoietic factor and cytotoxic T-cell differentiation factor) [2,3]. IL-6 signals through a receptor complex comprising IL-6Rα (CD126) and IL-6Rβ (CD130, glycoprotein 130 or gp130) and plays an important role in immune response, inflammation and hematopoiesis and in the endocrine and nervous systems [4,5].

The role of inflammation-supporting cytokines in cancer development and progression has recently become an active area in cancer research. As response rates in patients with advanced metastatic disease remain low with both standard chemotherapy and immunotherapy, novel approaches are being explored and cytokines have been proposed as potential therapeutic targets [6,7]. High levels of IL-6 in the tumor microenvironment, possibly reflecting the strong association between inflammation and cancer, have been found in almost all tumor types [3,8]. In addition, elevated serum concentrations of IL-6 correlate with worse prognosis in various cancers, including melanoma [9]. IL-6 plays a major role in the pathogenesis and development of malignancies, promotes tumor growth, inhibits apoptosis, induces angiogenesis and influences the overall metabolism in cancer patients [8–10]. In addition, IL-6 diminishes the effects of anticancer treatments by facilitating DNA repair and inducing antioxidant and anti-apoptotic effects in cancer cells. Therefore, blocking IL-6 or inhibiting its associated signaling alone or in combination with conventional anti-cancer therapies could be a potential therapeutic strategy in various cancers [10].

At present, targeting of IL-6 receptors (IL-6Rs) by monoclonal antibodies is an intensively studied therapeutic strategy [11–14]. Nevertheless, the inherent limitations of antibodies (e.g., high cost, invasive route of administration and high rate of immunogenicity) restrict their clinical usability [15]. The development of low-molecular-weight inhibitors is therefore highly desirable due to their superiority in in terms of oral absorption and low antigenicity. Despite the immense importance of this task and the efforts undertaken so far, only a few compounds are currently available [16–26].

Pentamethinium salts (PMSs) may represent an interesting structural motif for the design of new IL-6R inhibitors [3]. These compounds display mitochondrial accumulation [27–30] and potent cytotoxicity, which suggests their potential for use in cancer treatment [27,30–32]. For example, Krejci et al. reported that the cytotoxic effect of these compounds is associated with mitochondrial disintegration and metabolic collapse [30]. Thus, suitably designed PMSs could be used as dual anticancer agents targeting IL-6Rs and mitochondrial function simultaneously. This concept would effectively reflect the hypothesis that multitargeted therapeutic approaches capable of targeting/inhibiting more than one specific molecular target offer a promising strategy for anticancer treatment [33].

Nevertheless, the usability of PMSs can be significantly limited by their strong aggregation [27]. This could be overcome through a design based on imidazolium building blocks with higher charge density; e.g., PMS with two cationic charges. However, such a strategy may lead to a loss of cellular uptake and biological activity [28,31]. A possible solution could be Bis-PMSs, the charge density of which would lie in the interval between the values of mono- and doubly-charged PMS. Therefore, we designed, prepared and studied Bis-PMSs as potential cytostatic drugs with IL-6R inhibitory activity.

## 2. Materials and Methods

### *2.1. Synthesis of Bis-Pentamethinium Salts*

All chemicals and solvents were purchased from commercial suppliers (Merck/Sigma-Aldrich; Prague, Czech Republic and TCI Europe; Eschborn, Germany) and used without further purification. Nuclear magnetic resonance (NMR) spectra were recorded with a 500 MHz instrument (Bruker BioSpin, Billerica, MA, USA) at room temperature in DMSO-$d_6$ or $CDCl_3$. The chemical shifts (δ) are presented in ppm, the coupling constants (J) in Hz. The MestReNova program v 14.2 (Advanced chemistry development, Toronto, ON, Canada) was used to process the NMR spectra. High-resolution mass spectrometry (HRMS) spectra were obtained using electrospray ionization (ESI) with an LTQ Orbitrap spectrometer. Flesh chromatography on silica was used for isolation of target compounds.

**Preparation of *p*-bis-vinamidinium salt 1 [34–36]:** Phosphorus oxychloride (7 mL; 75 mmol) was added dropwise to dry DMF (15 mL) at 0 °C. The reaction mixture was stirred at room temperature for 30 min. Then, a solution of *p*-phenylenediacetic acid (2 g; 10 mmol) in DMF (7 mL) was added and the reaction mixture was stirred at 80 °C overnight.

The hot dark reaction mixture was then poured into crushed ice (ca. 200 mL), and a solution of sodium perchlorate (9.5 g; 78 mmol) in water (100 mL) was added to produce a precipitate. The solid was filtered, washed with water (3 × 75 mL) and vacuum-dried to obtain 5.01 g (95%) of a beige solid (1). $^{1}$H NMR (DMSO-$d_6$): δ 2.46 (s, 12H), 3.25 (s, 12H), 7.40 (s, 4H), 7.73 (s, 4H) ppm. $^{13}$C NMR (DMSO-$d_6$): δ 39.3, 48.7, 104.3, 132.2, 133.4, 163.0 ppm. HRMS (ESI$^+$): calcd for $C_{20}H_{32}N_4$ $[M]^{2+}$ 164.13080; found 164.13102; calcd for $C_{30}H_{32}Cl_2N_4O_4$ $[M + ClO_4]^+$ 427.21066; found 427.21078.

**Preparation of *m*-bis-vinamidinium salt 2 [37]:** Phosphorus oxychloride (7 mL; 75 mmol) was added dropwise to dry DMF (15 mL) at 0 °C. The reaction mixture was stirred at room temperature for 30 min. Then, a solution of *m*-phenylenediacetic acid (2 g; 10 mmol) in DMF (7 mL) was added and the reaction mixture was stirred at 80 °C overnight. The hot dark reaction mixture was then poured into crushed ice (ca. 200 mL), and a solution of sodium perchlorate (9.5 g; 78 mmol) in water (100 mL) was added to produce a precipitate. The solid was filtered, washed with water (3 × 75 mL) and vacuum-dried to obtain 4.59 g (87%) of a beige solid (2). $^{1}$H NMR (DMSO-$d_6$): δ 2.50 (s, 12H), 3.24 (s, 12H), 7.26 (s, 1H); 7.40 (d, 2H, J = 7.7 Hz), 7.51 (*t*, 1H, J = 7.6 Hz) ppm. $^{13}$C NMR (DMSO-$d_6$): δ 39.8, 48.5, 103.9, 128.5, 132.3, 133.4, 134.6, 163.3 ppm. HRMS (ESI$^+$): calcd for $C_{20}H_{32}N_4$ $[M]^{2+}$ 164.13080; found 164.13105; calcd for $C_{30}H_{32}Cl_2N_4O_4$ $[M + ClO_4]^+$ 427.21066; found 427.21082.

**Preparation of *p*-bis-malondialdehyde 3 [35,36]:** Vinamidinium salt 1 (1.47 g; 2.7 mmol) was added into an aqueous solution of sodium hydroxide (10% *w/w*; 10 mL) at 80 °C and the reaction mixture was stirred for 15 min (from suspension to yellow solution at the end). The reaction mixture was diluted with water (10 mL), cooled to ca. 5 °C and neutralized with 6 M hydrochloric acid to pH ≈ 5. Precipitated aldehyde was filtered, washed with water (20 mL) and vacuum-dried to obtain 518 mg (88%) of *p*-bis-malondialdehyde 3 as a white solid. $^{1}$H NMR (DMSO-$d_6$): δ 7.38 (s, 4H), 7.50 (bs, 4H), 12.10 (bs, 2H) ppm. $^{13}$C NMR (DMSO-$d_6$): δ 120.8, 128.3, 129.7, 188.0 ppm. HRMS (ESI$^+$): calcd for $C_{12}H_{11}O_4$ $[M + H]^+$ 219.06573; found 219.06532; calcd for $C_{12}H_{10}O_4Na$ $[M + Na]^+$ 241.04768; found 241.04737.

**Preparation of *m*-bis-malondialdehyde 4:** Vinamidinium salt 2 (1.47 g; 2.7 mmol) was added into an aqueous solution of sodium hydroxide (10% *w/w*; 10 mL) at 80 °C and the reaction mixture was stirred for 15 min (from suspension to yellow solution at the end). The reaction mixture was cooled to ca. 5 °C and neutralized with 1 M hydrochloric acid to pH ≈ 5. The mixture was left in the fridge overnight, and the precipitated aldehyde was then filtered, washed with water (20 mL) and vacuum-dried to obtain 301 mg (51%) of *m*-bis-malondialdehyde 4 as a beige solid. $^{1}$H NMR (DMSO-$d_6$): δ 7.25 (m, 3H), 7.51 (s, 1H), 8.51 (bs, 4H), 10.25 (bs, 2H) ppm. $^{13}$C NMR (DMSO-$d_6$): 121.1, 126.8, 127.5, 130.0, 130.8 ppm. HRMS (ESI$^+$): calcd for $C_{12}H_{11}O_4$ $[M + H]^+$ 219.06573; found 219.06529; calcd for $C_{12}H_{10}O_4Na$ $[M + Na]^+$ 241.04768; found 241.04738.

**Preparation of *p*-bis-pentamethinium salt 5 from *p*-bis-vinamidinium salt 1:** The compound was prepared using a slightly modified procedure described in the literature [34]. *p*-Bis-vinamidinium salt **1** (210 mg; 0.4 mmol), 1,2,3,3-tetramethyl-3H-indol-1-ium iodide (602 mg; 2 mmol) and potassium iodide (664 mg; 4 mmol) were mixed in anhydrous ethanol (6 mL). DIPEA (0.35 mL; 2 mmol) was added and the reaction mixture was stirred at 75 °C overnight. After cooling down, volatile compounds were removed under reduced pressure and the residue was purified using flash chromatography (dichloromethane/methanol, gradient from 98:2 to 90:0, *v/v*). *p*-Bis-pentamethinium salt **5** was obtained as a deep greenish-blue solid in a yield of 26 mg (6%).

**Preparation of *p*-bis-pentamethinium salt 5 from *p*-bis-malondialdehyde 3:** *p*-Bis-malondialdehyde **3** (44 mg, 0.2 mmol) and 1,2,3,3-tetramethyl-3H-indol-1-ium iodide (301 mg, 1 mmol) were mixed in *n*-butanol (15 mL). The reaction mixture was stirred at 115 °C overnight. After cooling down, volatile compounds were removed under reduced pressure and the residue was purified using flash chromatography (dichloromethane/methanol, gradient from 98:2 to 90:0, *v/v*). *p*-Bis-pentamethinium salt **5** was obtained as a deep greenish-blue solid in a yield of 79 mg (36%). $^{1}$H and $^{13}$C data were in accordance

with the published data [34]. HRMS (ESI$^+$): calcd for $C_{60}H_{64}N_4$ $[M]^{2+}$ 420.25600; found 420.25605; calcd for $C_{60}H_{64}IN_4$ $[M + I]^+$ 967.41702; found 967.41655.

**Preparation of *m*-bis-pentamethinium salt 6 from *m*-bis-vinamidinium salt 2:** The compound was prepared using a slightly modified procedure described in the literature [34]. *m*-Bis-vinamidinium salt 2 (210 mg; 0.4 mmol), 1,2,3,3-tetramethyl-3H-indol-1-ium iodide (602 mg; 2 mmol) and potassium iodide (664 mg; 4 mmol) were mixed in anhydrous ethanol (6 mL). DIPEA (0.35 mL; 2 mmol) was added and the reaction mixture was stirred at 75 °C overnight. After cooling down, volatile compounds were removed under reduced pressure and the residue was purified using flash chromatography (dichloromethane/methanol, gradient from 98:2 to 90:0, *v/v*). *m*-Bis-pentamethinium salt 6 was obtained as a deep greenish-blue solid in a yield of 22 mg (5%).

**Preparation of *m*-bis-pentamethinium salt 6 from *m*-bis-malondialdehyde 4:** Malondialdehyde 4 (44 mg, 0.2 mmol) and 1,2,3,3-tetramethyl-3H-indol-1-ium iodide (301 mg, 1 mmol) were mixed in *n*-butanol (15 mL). The reaction mixture was stirred at 115 °C overnight. After cooling down, volatile compounds were removed under reduced pressure and the residue was purified using flash chromatography (dichloromethane/methanol, gradient from 98:2 to 90:0, *v/v*). *m*-Bis-pentamethinium salt 6 was obtained as a deep greenish-blue solid in a yield of 59 mg (27%). $^1$H NMR ($CDCl_3$): δ 1.78 (s, 24H), 3.56 (s, 12H), 5.82 (d, J = 14.0 Hz, 4H), 7.27 (m, 17H), 7.46 (d, J = 7.7 Hz, 2H), 7.82 (*t*, J = 7.7 Hz, 1H), 8.21 (d, J = 14.1 Hz, 4H) ppm. $^{13}$C NMR ($CDCl_3$): δ 28.2, 33.2, 49.8, 101.0, 111.6, 122.2, 125.7, 129.0, 130.2, 130.8, 131.7, 133.7, 136.3, 140.8, 142.7, 153.1, 173.9 ppm. HRMS (ESI$^+$): calcd for $C_{60}H_{64}N_4$ $[M]^{2+}$ 420.25600; found 420.25616; calcd for $C_{60}H_{64}IN_4$ $[M + I]^+$ 967.41702; found 967.41630.

### *2.2. Analytical Studies*

Spectral characteristics in the range of 300 to 800 nm were obtained using a Shimadzu UV-2401 PC UV/VIS spectrometer. The Bis-PMSs were measured in four solvents (DMSO, methanol, ethanol and phosphate buffer). Both Bis-PMSs **5** and **6** were first dissolved in 1 mM DMSO stock solution, which was diluted to a final concentration of 1 μM, and measured in a classical 1 cm PMMA cuvette.

The fluorescence properties of the compounds were measured using a FLS1000 modular fluorescence spectrometer (Edinburgh Instruments, Livingston, UK). The substances were dissolved in DMSO and diluted to a final concentration of 500 nM. The measurements were carried out in a Fluorescence Quartz Cuvette Cell with 1 cm length for the absorbent layer. The excitation and emission maxima of Bis-PMSs **5** and **6** are provided in Table S1.

### *2.3. Photostability Assay*

The photostability of the fluorescent probes was tested in the BJ-hTERT cell line. The cells (10,000 cells per well) were seeded in 35 mm glass-bottom dishes in complete culture media and allowed to adhere for 24 h. When the cells had reached the desired confluence, the medium was removed and the cells were washed twice with PBS and incubated in Dulbecco's Modified Eagle's Medium (DMEM), lacking phenol red and containing bis-pentamethinium salts **5** and **6** (at 100 nM) and MT-G (100 nM) or MT-R (100 nM), for 30 min under standard conditions.

The excitation wavelength was 630 nm and the emission was recorded in the 650–670 nm range. For MT-G, the excitation wavelength was 490 nm and the emission was measured in the 510–550 nm range. MT-R was excited at 581 nm and the emission was recorded in the 640–650 nm range. Exposure time was 5 min.

### *2.4. In Silico Docking of Bis-Pentamethinium Salts 5 and 6 to the IL-6R Model*

The 3D structural model of the human interleukin 6 receptor (IL-6R) was generated from the crystallographic structure of the complex between IL-6 and its receptor (IL-6R-α and IL-6R-β, PDB id 1P9M) by editing out the coordinates of the IL-6 molecule. All bound water molecules and ligands were removed.

Bis-PMSs **5** and **6** and a mono penthamethinium salt with a phenyl group in the γ-position were docked to the IL-6R using the CB-Dock web server [38]. All docking poses from this cavity (binding site) were visually inspected with BIOVIA Discovery Studio Visualiser [39], and 2D interaction diagrams and 3D visualizations of the protein–ligand complex were generated and are presented.

### *2.5. Microscale Thermophoresis (MST)*

Microscale thermophoresis (MST) measurements were performed with a Monolith NT.115 device (Nano Temper Technologies GbmH, installed at the Centre of Molecular Structure, BIOCEV, with access granted through CIISB). The binding affinities of Bis-PMSs **5** and **6** to the IL-6R receptor molecule (Bio-Techne R&D Systems, Minneapolis, MN, USA; containing α and β subunits) were measured in PBS buffer (pH 7.4). Sixteen-step dilution was performed by adding 20 μL of IL-6R at twice the concentration (10 μmol/L) to the first PCR tube, and 10 μL of buffer (PBS, pH = 7.4) was added to PCR tubes 2–16. Then, we transferred 10 μL of the ligand from PCR tube 1 to PCR tube 2 and mixed the content by pipetting up and down multiple times. We repeated this procedure for tubes 3–16 and discarded the last 10 μL from PCR tube 16. The first capillary contained the highest concentration of the ligand (e.g., IL-6R) and the last capillary (number 16) contained the lowest concentration of the ligand. Ten μL of each Bis-PMS (**5** or **6)** in PBS buffer with 1% of DMSO and 0.005% of Pluronic was added to each PCR tube and mixed by pipetting up and down. The final concentration of Bis-PMS (**5** and **6**) was 100 nmol/L. We loaded solutions from each PCR tube into NT.115 Standard Capillaries, and scanning was performed using 20% LED power and 40% MST power. Data were analyzed using Nano Temper Technologies' NT Analysis 1.5.41 software (Technologies GmbH; München, Deutschland).

### *2.6. Cell Lines and Cell Culture*

Cells were cultured under standard conditions in a humidified atmosphere of 5% $CO_2$ in air at 37 °C. Normal dermal fibroblasts (HF-P4) were derived from residuary skin specimens of healthy persons who underwent plastic surgery at the Department of Plastic surgery, Third Faculty of Medicine, Charles University and University Hospital Královské Vinohrady, Prague, Czech Republic, as described by Szabo et al., 2011 and Dvořánková et al., 2019 [9,10]. Informed consent from the patients and the approval of the Local Ethical Committee, in agreement with the Helsinki Declaration, were obtained. hTERT-immortalized foreskin fibroblast cell line **BJ-hTERT** (ATCC CRL-4001) was cultured in Dulbecco's Modified Eagle's Low-Glucose Medium, supplemented with 10% FBS, 0.01% non-essential amino acids (NEAAs), 100 U/mL penicillin and 100 μg/mL streptomycin. Human skin melanoma cell line **A-2058**, derived from a lymph node metastasis (ATCC CRL-11147, Manassas, VA, USA), and the highly metastatic **BLM** melanoma cell line (obtained from L. van Kempen and H. Van Krieken, Department of Pathology, Radboud University, Nijmegen, The Netherlands) were cultured in Dulbecco's Modified Eagle's Medium (DMEM) supplemented with 10% FBS, 100 U/mL penicillin and 100 μg/mL streptomycin. The osteosarcoma **U-2 OS** cell line (ATCC HTB-96) was cultured in McCoy's 5a modified medium supplemented with 10% FBS, 100 U/mL penicillin and 100 μg/mL streptomycin. The non-small cell lung human carcinoma **H1299** cell line (ATCC CRL-5803) was cultured in RPMI-1640 medium supplemented with 10% FBS, 100 U/mL penicillin and 100 μg/mL streptomycin. Human breast tumor cell line **BT-20** (ATCC HTB-19) was cultured in Eagle's Minimum Essential Medium (EMEM) supplemented with 10% FBS, 100 U/mL penicillin and 100 μg/mL streptomycin. Human (**U251MG**, Cell Lines Service GmbH, Eppelheim, Germany) and mouse (**Gl261**, Division of Cancer Treatment and Diagnosis Tumor repository, National Cancer Institute, Bethesda, MD, USA) glioblastoma cell lines were propagated in Dulbecco's Modified Eagle's Medium (DMEM) and RPMI-1640, respectively, supplemented with 10% of fetal bovine serum (FBS).

### *2.7. Cytotoxicity Assays*

A colorimetric MTT cell metabolic activity assay was used to determine the cytotoxicity of Bis-PMSs **5** and **6**. For these experiments, the HF-P4, BJ-hTERT, BLM, A-2058, U-2 OS, H1299 and BT-20 cells were cultured under standard conditions (37 °C, humidified atmosphere with 5% $CO_2$ in air) in culture medium (DMEM, RPMI-1640, McCoy's or EMEM with 10% FBS). Cells were plated in 96-well plates at a density of 5000 cells per well and grown for 24 h. The medium was then replaced with a medium containing Bis-PMSs **5** and **6**, and cells were cultured for an additional 48 h. Afterwards, the medium was exchanged for medium with the MTT yellow tetrazolium dye (3-(4,5-dimethylthiazol-2-yl)-2,5-diphenyltetrazolium bromide, Sigma-Aldrich) and incubated for 2 h at 37 °C. After that, the yellow tetrazole dye was removed and DMSO was used to dissolve the reduced purple formazan formed in living cells. The absorbance of the converted dye was measured at a wavelength of 570 nm with the reference of 630 nm using a SpectraMax ABS Plus microplate reader (Molecular Devices). Experiments were performed in quadruplicate and repeated three times with similar results. In U251MG and GL261 cells, an assay assessing cell growth independent of mitochondrial respiration was used [40]. Cells were plated in 96-well plates at a density of 5000 cells per well and grown for 24 h under standard conditions in culture medium (DMEM and RPMI-1640 with 10% FBS for U251MG and Gl261 cells, respectively). The medium was then replaced by that supplemented with Bis-PMSs **5** and **6**. After 72 h of exposure, surviving cells were fixed and stained with methylene blue (5 g/L in 50%, *v/v*, ethanol) and lysed with 1% sodium dodecyl sulfate, and the relative cell number was determined by reading absorbance at 630 nm using a 96-well plate reader (Sunrise; Tecan, Männedorf, Switzerland).

The cell inhibitory concentration (IC) was calculated using the equation IC = ($A_{PMS}$ well/mean $A_{control}$ wells) × 100%. The half-maximal inhibitory concentration ($IC_{50}$) was calculated from dose–response curves using GraphPad Prism software (v. 8.0.1, La Jolla, CA, USA). The selectivity indexes towards cancer cells were calculated as a ratio of the average of the $IC_{50}$ values for HF-P4 and BJ-hTERT human fibroblasts and the $IC_{50}$ value for the corresponding cancer cell line. For U251MG and Gl261 glioblastoma cells, the cytoselectivity was calculated against normal HF P4 fibroblast cells, which were analyzed using the same cytotoxicity assay.

### *2.8. Intracellular Studies of Bis-Pentamethinium Salts*

Intracellular localization of Bis-PMSs **5** and **6** in living cells was investigated at 37 °C and 0.05 $CO_2$ tension using a Leica TCS SP8 WLL SMD-FLIM confocal microscope equipped with an HC PL APO CS2 63x/1.2 W water immersion objective. Glass bottom dishes (dish size 35 mm, well size 20 mm), especially designed for high-resolution imaging, were used. Human dermal fibroblast cells (HF-P4—primary cell culture or BJ-hTERT cell line), melanoma cells (A-2058, BLM), osteosarcoma cells (U-2 OS), non-small cell lung cancer cells (H1299) and breast cancer cells (BT-20) were applied to the glass bottom dishes at a density of 10,000 cells per well. All cells were kept under standard culture conditions in culture medium (DMEM, RPMI-1640, McCoy's or EMEM with 10% FBS). When the cells reached the desired confluence (after 24 h), the medium was removed from the dish and the cells were rinsed twice with PBS and further incubated for 30 min in complete culture medium supplemented with the Bis-PMS at a concentration of 100 nM. A commercially available organic fluorescent probe, MitoTracker™ Green FM (ThermoFisher Scientific, Waltham, MA, USA), was used to label mitochondria. This green fluorescent dye was added at 300 nM concentration to the cells, which were then incubated for 30 min under standard growth conditions. After removal from the incubator, the cells were washed twice with PBS and analyzed. For the measurements, the excitation wavelength was 630 nm and the emission was measured in the 650–670 nm range. The MitoTracker™ Green FM dye was excited at 490 nm and the emission was recorded in the 510–550 nm wavelength range.

For electron microscopy, control HFP4 and melanoma A2058 cells, as well as cells exposed to 5 μM Bis-PMS **5** or **6** for 2 h, were routinely processed. Briefly, cells were

fixed with 2.5% glutaraldehyde in 0.1 M Sörensen´s sodium-potassium phosphate buffer at pH 7.2–7.4 (all Thermo Fisher Scientific, Waltham, MA, USA). After washing, the cells were postfixed in 1% osmium tetroxide, dehydrated with a series of acetone (Lach-Ner, Neratovice, Czech Republic) and embedded in Epon-Durcupan resin (Sigma-Aldrich, St. Louis, MO, USA). Then, 80 nm ultrathin sections were prepared using an Ultramicrotome Leica EM UC6 (Leica Microsystems, Wetzlar, Germany) with a diamond knife (Diatome, Biel, Switzerland). The sections were mounted on 200 mesh size copper grids and examined in a JEOL JEM-1400 Flash transmission electron microscope operated at 80 kV equipped with a Matataki Flash sCMOS camera (JEOL, Akishima, Tokyo, Japan).

### *2.9. Colocalization Analysis*

Colocalization analysis was performed in Fiji-Image J software using images of cells exposed to Bis-PMSs **5** and **6** and MitoTracker™ Green FM. The correlation between fluorescence intensities in the green and red channels was evaluated using Pearson's correlation coefficient.

### *2.10. Mitochondrial Respiration*

Mitochondrial respiration and extracellular acidification rate were measured in an Agilent Seahorse XF Analyzer (XF24, Agilent, Prague, Czech Republic) following Zdrazilova et al. [41], with two slight modifications. First, bis-pentamethinium salts **5** and **6** were added to cells in concentrations of 1 and 5 μM each—always into four wells on the day after seeding—and were incubated for two hours. Second, 50 μL of glucose (final assay concentration 10 mM) was added to Cartridge port A, 55 μL oligomycin (final assay concentration 1.5 μM) to port B, 61 μL FCCP (final assay concentration 0.6 μM) to port C and 67 μL rotenone with antimycin A and 2-deoxy-D-glucose (final assay concentrations 2 uM, 1 μM and 100 mM) to port D.

### *2.11. Inhibitory Effect of Bis-PMSs 5 a 6 on STAT3 Activation in a HEK Reporter Cell Line*

Reporter cells (HEK-Blue™ IL-6 Cells (InvivoGen, San Diego, CA, USA); 10,000 cells per well in a 96-well plate) were seeded in DMEM with 10% heat-activated FBS (56 °C for 30 min to inactivate the alkaline phosphatase activity) and allowed to fully adhere for 48 h.

After 48 h, the medium was changed. All experiments were performed in three technical replicates. The tested concentrations of Bis-PMSs **5** and **6** in the culture medium were 10, 5, 1 and 0.5 μM. After 2 h (time to inhibit the receptor complex), recombinant human IL-6 (10 ng/mL) was added, and cells were further cultured in an incubator at 37 °C and 5% $CO_2$ for 24 h. Tocilizumab (20 ng/mL) in the culture medium was used as a control inhibitor under otherwise identical conditions.

After 24 h of incubation with IL-6, a 20 μL sample was taken from each well following a brief agitation of the culture plate (on a shaker). The sample was mixed with 180 μL of QuantiBlue substrate to quantity the activity of secreted embryonic alkaline phosphatase (SEAP). The optical density (absorbance) of the color product was measured using a microplate reader (SpectrMax iD3 spectrophotometer at 635 nm) after 30 min at 37 °C.

## 3. Results and Discussion

### *3.1. Synthesis of Bis-Pentamethinium Salts*

Generally, pentamethinium salts can be prepared by reaction of quaternary salts of nitrogen heterocycles containing an active methyl (e.g., *N*-alkylated 2,3,3-trimethyl-3H-indol-1-ium, 2-methylbenzothiazol-3-ium, 2-methylbenzoxazol-3-ium, 2- or 4-methylquinolin-1-ium salts) with malondialdehydes or with vinamidinium salts [28,29,31,34,42–44].

The synthesis of Bis-PMS is shown in Figure 1. The initial *p*- and *m*-phenylenediacetic acid was reacted with phosphorus oxychloride in DMF to yield the bis-vinamidinium salts **1** and **2** [34–36]. Bis-vinamidinium salts were isolated as perchlorates in 87–95% yields. In the next step, bis-vinamidinium salts **1** and **2** were hydrolyzed by aqueous sodium hydroxide to give corresponding bis-malondialdehydes in 51–88% yields [36]. In the last

step, bis-malondialdehydes **3** and **4** were reacted with 1,2,3,3-tetramethyl-3H-indol-1-ium iodide to give target Bis-PMSs **5** and **6** in 27–36% yields. Alternatively, target Bis-PMSs **5** and **6** were prepared by reaction of vinamidinium salts **1** and **2** with 1,2,3,3-tetramethyl-3H-indol-1-ium iodide in 5–6% yields. [36] In all cases, reactions with *m*-derivatives gave products (compounds **2**, **4,** and **6**) in lower yields compared to *p*-derivatives.

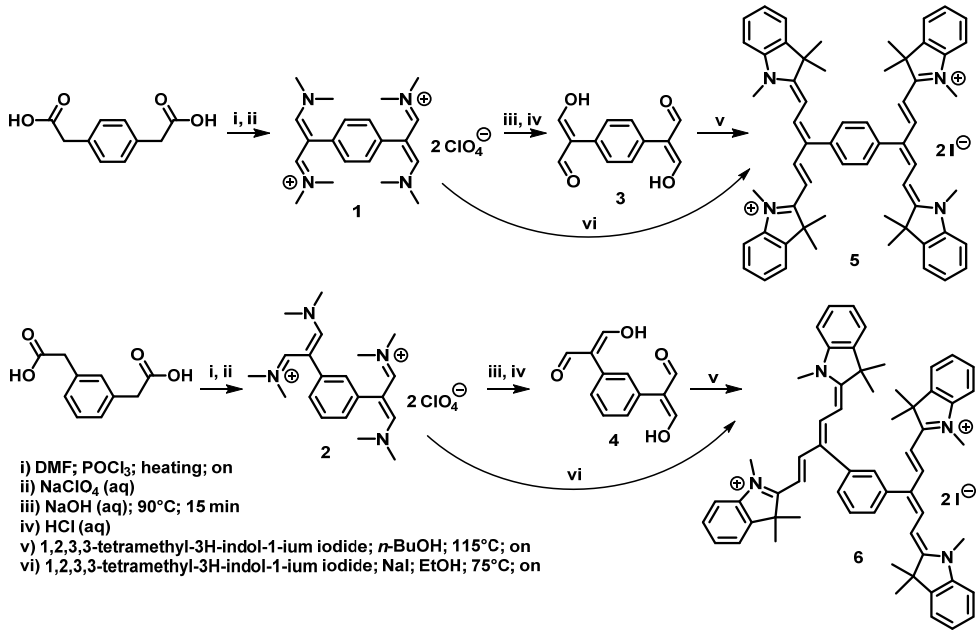


**Figure 1.** Synthesis of Bis-PMSs **5** and **6** overnight (on).

### *3.2. Photophysical Characteristics*

The spectral characteristics of Bis-PMSs **5** and **6** were obtained using UV/VIS and fluorescent spectrometric studies. Both salts were measured in four different solvents: dimethyl sulfoxide (DMSO), ethanol, methanol and phosphate-buffered saline. Absorption and fluorescence spectra are shown in Figure 2 and Figures S1–S3 and the resulting values for the excitation and emission maxima are provided in Table S1.

Both Bis-PMSs had absorption/excitation maxima in the purple area of the visible spectrum (600–640 nm) and emission maxima in the red area (650 to 670 nm). The meta derivative (Bis-PMS **6**) showed higher fluorescence intensity at the wavelength of the emission maxima compared to the para derivative, Bis-PMS **5** (Figure 2). These characteristics were similar to mono-substituted indolium pentamethinium salts. For example, a DMSO solution of a pentamethinium salt with pyrimidine substitution in the γ-position displayed an absorption maximum at 643 nm, an emission maximum at 655 nm and an excitation maximum at 641 nm [28].

Stability of Bis-PMS **5** and PMS **6** in cell cultivation medium (EMEM) simulating physiological conditions was evaluated using UV-Vis spectroscopy. Both compounds, especially Bis-PMS 5, displayed significant spectral change over time (Figures S4 and S5), which could imply their possible chemical instability in aqueous solutions, most probably their hydrolysis. Nevertheless, this effect was strongly repressed in the presence of MeOH (another protic solvent), which demonstrated that the observed spectral change was not caused by hydrolysis but most probably by interaction with media components, such as anions, and/or aggregation of the compounds. UV-Vis spectra in methanol and phosphate buffer, which represent monomer and aggregate forms of polymethinium salts, are shown in Figure S1. Similar spectral behavior was previously observed for mono pentamethinium salts [27–29,31,45–47].

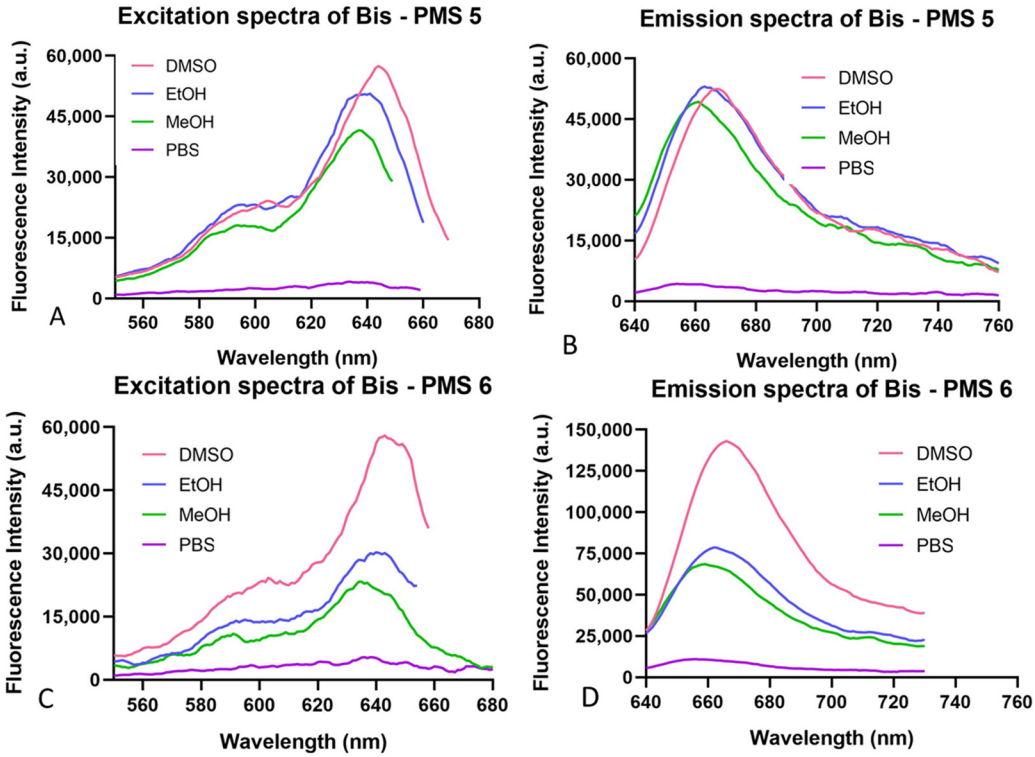


**Figure 2.** Excitation (**A**,**C**) and emission (**B**,**D**) spectra of Bis-PMSs **5** and **6** in four different solvents (DMSO, EtOH, MeOH and phosphate-buffered saline).

The photostability of Bis-PMSs **5** and **6** was similar to MitoTracker™ Green FM and significantly better than MitoTracker™ Red FM (Figure S6).

### *3.3. In Silico Docking of Bis-Pentamethinium Salts **5** and **6** to the IL-6R Model*

For the docking studies, we used a structural model of IL-6R consisting of IL-6Rα and IL-6Rβ (gp130) subunits without IL-6 (pid 1P9M). Bis-PMSs 5 and 6 were docked to the IL-6R using the CB-Dock web server [38]. All docking poses from the protein binding site were visually inspected with BIOVIA Discovery Studio Visualiser [39], and 2D interaction diagrams and 3D visualizations of the protein–ligand complex were generated and are presented (Figure 3). The binding model suggests that both Bis-PMSs **5** and **6** bind to the IL-6Rβ subunit responsible for signal transduction after IL-6 binding [48]. A similar mechanism was observed for other low-molecular-weight inhibitors of IL-6 signaling, such as madindoline [24]. The computed values of the free energy of binding between Bis-PMSs **5** and **6** and IL-6R were −9.5 and −8.1 kcal/mol, respectively, which suggests a strong affinity in both compounds for the IL-6R and, thus, possible inhibitory activity towards IL-6R signaling.

Docking studies suggest that both compounds bind to IL-6R via their interaction with Phe69, Ile52, Ile77, Ala73 and Phe50. Nevertheless, we found a significant difference in the mode of interaction (Table S2). For example, Bis-PMS **5** forms an alkyl bond with Ile52 and Ile77 through its methyl group. The methyl group of Bis-PMS **6** forms an alkyl bond with Ile77; however, IL77 also interacts via alkyl-π bond with the methinium chain. Ile52 forms a π-alkyl bond with the benzene imidazolium group. Bis-PMS **5** interacts with Phe69 (π-aliphatic bond with methyl groups) and Phe50 (π-bond with the benzene imidazolium group and π-alkyl bond with the methyl group). In the case of Bis-PMS **6**, Phe50 interacts with two imidazolium benzene groups via π-sigma and π-alkyl with the methyl group and methinium chains, respectively. Similarly, the phenyl group of Phe50 π stacks and forms a π-alkyl bond with the imidazolium benzene and methyl groups, respectively.

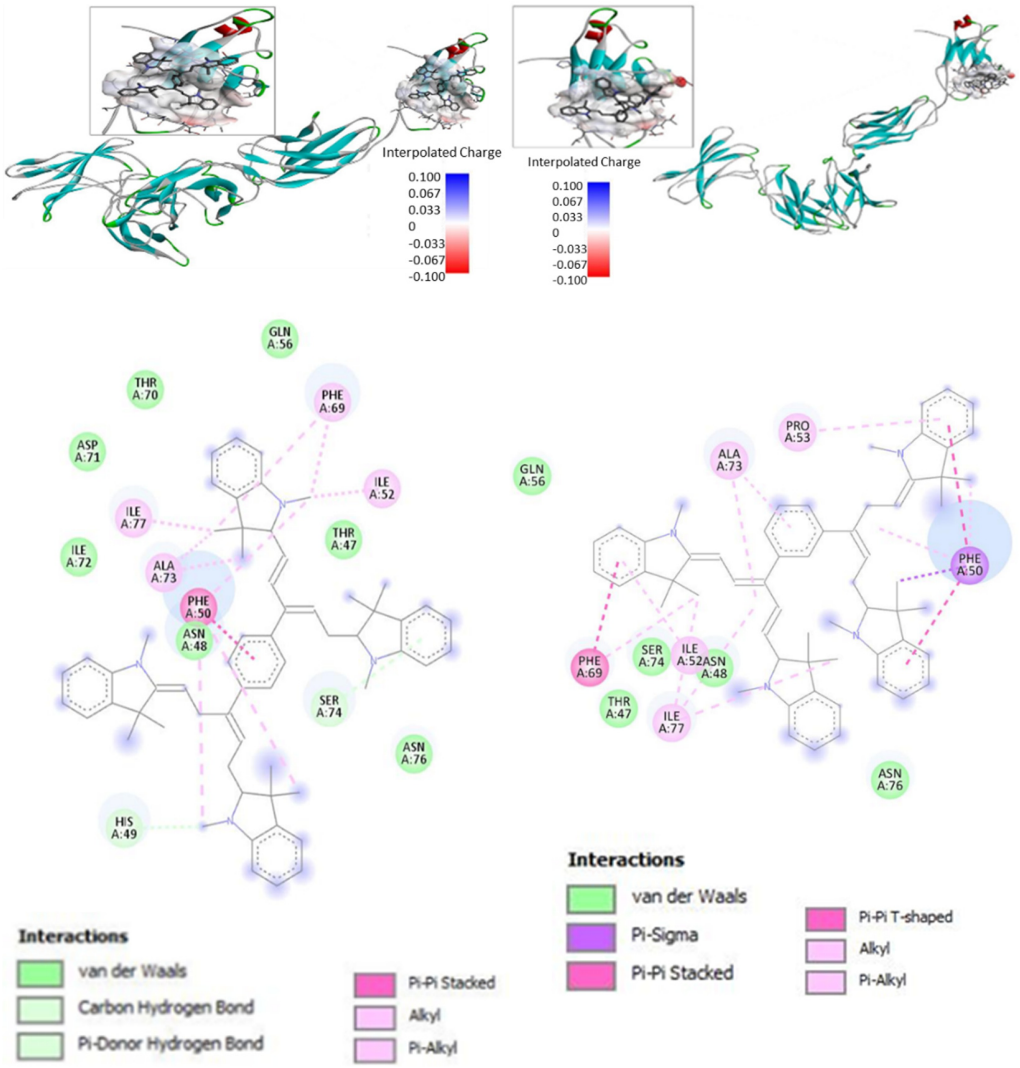


**Figure 3.** Docking of Bis-PMSs **5** and **6** to the IL-6 receptor (IL-6R) containing α and β subunits. Upper panels show a 3D model of IL-6R; the binding site (cavity) is localized in IL-6Rβ. Electron density in the binding site is shown as a color scale from blue (**low**) to red (**high**). Lower panels show the interaction of Bis-PMSs **5** and **6** with the amino acid residues of a homology model of IL-6R. Bis-PMS **5** and **6** docked to the IL-6R, −9.5 and, −8.1 kcal/mol, respectively.

Furthermore, only the methyl group of Bis-PMS **5** interacts with Asn48 (alkyl bond) and His49 (π donor hydrogen bond). On the other hand, Bis-PMS **6** exclusively interacts with Pro53 (π-alkyl with the benzene imidazolium group). This suggests that the para structure motif of **5** could be more suitable for the binding of IL-6R. In this case, its shift to the meta-structure motif represented by Bis-PMS **6** leads to significantly reduced binding (binding energy −9.5 vs. −8.1 kcal/mol). For comparison, the value of binding energy obtained from docking of a mono pentamethinium salt with a phenyl group in the γ-position (Figures S7 and S8) was −8.3. kcal/ mol.

### *3.4. Interaction of Bis-Pentamethinium Salts 5 and 6 with IL-6R*

The ability of Bis-PMS **5** and **6** to bind to the IL-6R protein containing α and β subunits was assessed by microscale thermophoresis (Figure 4). We processed the temperature jump (T-jump) defined as the fluorescence change induced by sample heating before the thermophoretic molecule transport sets in. T-jump allows the quantification of the affinity of interaction from changes in the intrinsic temperature dependence of the fluorescence.

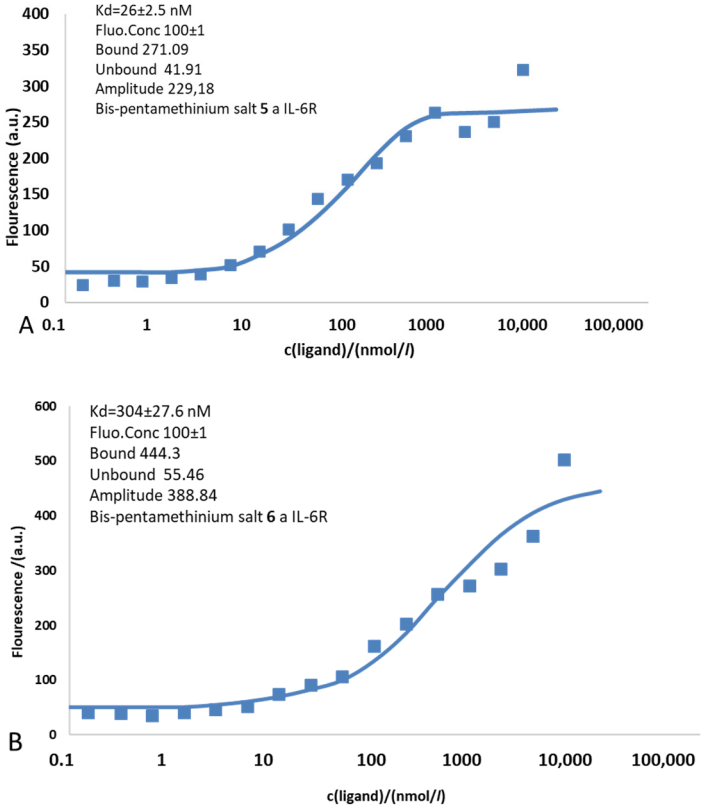


**Figure 4.** Binding of Bis PMS to the IL-6 receptor (IL-6R) containing α and β subunits evaluated by a microscale thermophoresis assay. The binding isotherm of Bis-PMSs **5** (**A**) and **6** (**B**) resulting from plotting the difference in normalized fluorescence against the concentration of the non-fluorescent binding partner (ligand–IL-6R).

The experimentally determined dissociation constants for Bis-PMSs **5** and **6** were 26.5 ± 2.5 nM and 304 ± 27.6 nM, respectively, which agreed with the docking results (see the in silico data above). In accordance with our expectations (based on the value of interaction energy), higher affinity for the IL-6R was observed for Bis-PMS **5**. Nevertheless, the values in both compounds suggest their strong potential for IL-6R inhibition. For comparison, tocilizumab (the antibody used in clinical practice) binds Il-6R with a significantly higher affinity (Kd = 2.54 ± 0.12 nM) [49], and values previously reported for synthetic inhibitors, such as chikusetsusaponin inhibitors, are several times higher compared to Bis-PMS **5** and **6** [50]. In line with this, we observed a strong inhibitory effect of tocilizumab on IL-6-induced STAT3 activation in IL-6 reporter cells and a mild effect of nontoxic concentrations of Bis-PMSs **5** and **6** (Figure S9). Thus, our data imply that the Bis-PMS scaffold is a promising novel structure motif for the inhibition of IL-6R signaling.

### *3.5. Cytotoxicity Assays*

The cytotoxic activities of Bis-PMSs **5** and **6** were evaluated in normal (HF-P4 and BJ-hTERT fibroblasts) and malignant (BLM, A-2058, U-2 OS, H1299, BT-20) cells using a conventional MTT viability assay. For the measurements, cells were exposed to 0–10 μM of Bis-PMSs **5** and **6** under standard conditions in a complete cell culture medium and cell viability was measured after 48 h of treatment. In addition, cytotoxicity was tested in U251MG and Gl261 glioma cells using an assay that assesses cell growth independent of mitochondrial respiration [40] (Figures S10 and S11 and Table S3). The mean $IC_{50}$ values are shown in Table 1 and Figure S12. The cytoselectivity index for cancer cell lines is shown in Figure 5.

**Table 1.** Cytotoxicity of Bis-PMSs **5** and **6** in normal and cancer cells. $IC_{50}$ (μmol/L) of Bis-PMSs **5** and **6** was determined in HF-P4 and BJ-hTERT human fibroblasts, BLM and A2058 human melanoma cells, H1299 human non-small cell lung cancer cells, human BT-20 breast cancer cells, human U251MG and mouse Gl261 glioblastoma cells and U2-OS human osteosarcoma cells.

| Cell Lines | Bis-PMS 5 | | Bis-PMS 6 | |
|---|---|---|---|---|
| | Mean (μM) | SD | Mean (μM) | SD |
| **HFP4** | 0.987 | 0.575 | 1.499 | 0.452 |
| **BJ-hTERT** | 1.660 | 0.038 | 1.218 | 0.442 |
| **BLM** | 0.300 | 0.117 | 1.419 | 0.486 |
| **A2058** | 0.287 | 0.109 | 0.636 | 0.359 |
| **H1299** | 2.755 | 0.063 | 0.169 | 0.031 |
| **BT-20** | 0.701 | 0.228 | 0.779 | 0.160 |
| **U2-OS** | 0.496 | 0.145 | 0.242 | 0.092 |
| **U251** | 0.719 | 0.219 | 0.505 | 0.020 |
| **Gl261** | 0.971 | 0.079 | 0.268 | 0.050 |

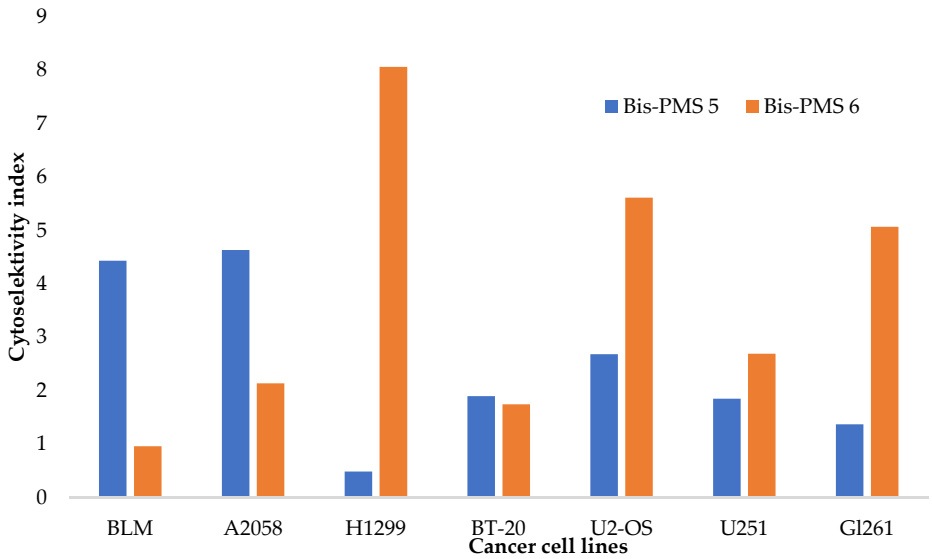


**Figure 5.** Cytoselectivity of Bis-PMSs **5** (blue) and **6** (orange) for cancer cell lines (BLM and A2058 human melanoma cells, H1299 human non-small cell lung cancer cells, human BT-20 breast cancer cells and U2-OS human osteosarcoma cells) against normal cells (HF P4 and BJ-hTERT human fibroblasts). For U251MG and Gl261 glioblastoma cells, the cytoselectivity was calculated against normal HF P4 fibroblast cells, which were analyzed using the same cytotoxicity assay.

Bis-PMS **6** exhibited higher toxicity in most tested cell lines (Table 1). The cellular viability of cancer cells was 80% and less after 48 h of incubation with the compound at >0.5 μM in the majority of cell lines. For comparison, the $IC_{50}$ of mono pentamethinium salts evaluated in previous studies was comparable [28]. These results suggest the cytotoxicity of the tested compounds against a broad spectrum of cancer cells representing various tumor types. Nevertheless, there was substantial toxicity towards normal cells as well.

### *3.6. Influence of Bis-Pentamethinium Salts 5 and 6 on Mitochondrial Morphology and Function*

PMS as hydrophobic cations are usually localized in mitochondria [27–29]. They can display strong cytotoxic effects against cancer cells closely associated with alterations of the mitochondrial metabolism [30].

Localization of the Bis-PMSs **5** and **6** was studied in normal fibroblasts (a primary cell culture HF-P4 and a cell line BJ-hTERT), two melanoma cell lines (BLM and A-2058), an osteosarcoma cell line (U-2 OS) and a non-small cell lung cancer cell line (H1299). No obvious cell morphology or viability changes were observed with the used concentration

(100 nM). Both Bis-PMSs **5** and **6** displayed a nearly exclusive mitochondrial localization (Figures 6, S13 and S14), as demonstrated by an almost complete overlap of their fluorescence signal and the fluorescence signal of the specific commercial mitochondrial probe MitoTracker Green (MT-G) (correlation coefficients (r) between 0.94 and 0.98; Figure S15).

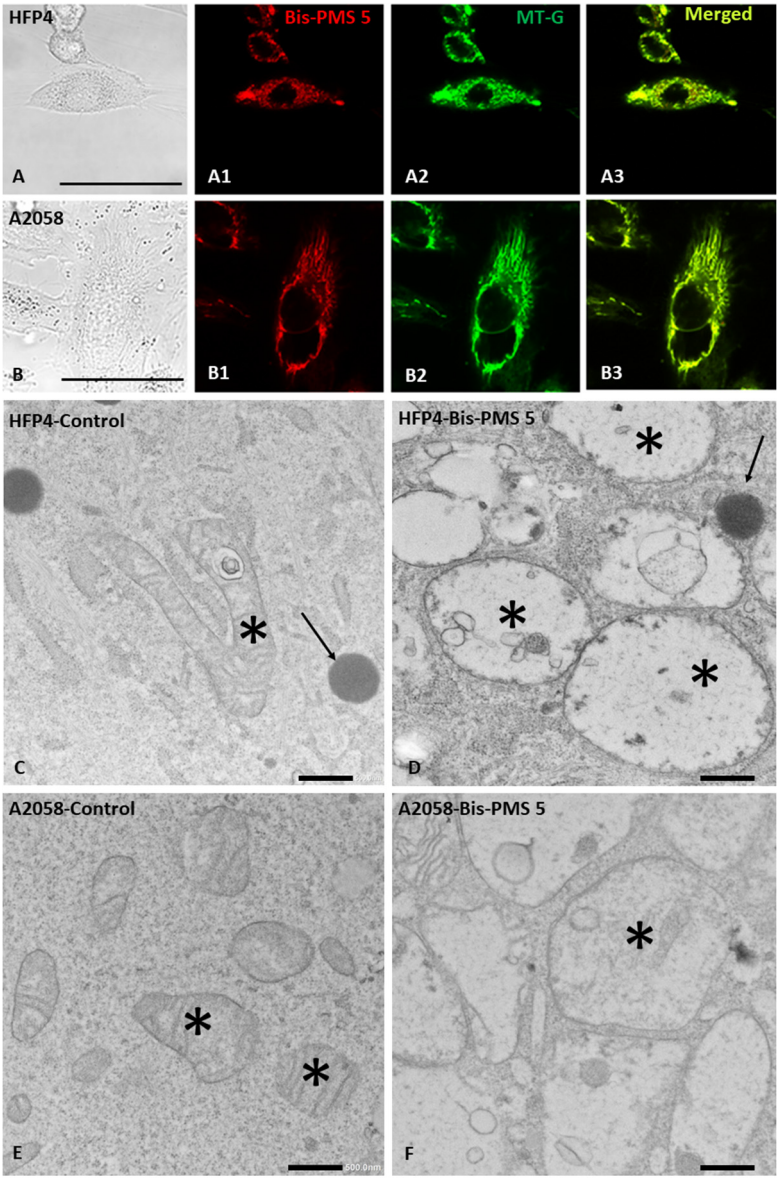


**Figure 6.** Influence of Bis-PMS **5** on normal HFP4 fibroblast (**A**,**C**,**D**) and A2058 melanoma cells (**B**,**E**,**F**). Subcellular localization of Bis-PMS 5 can be seen in the red channel (λex = 630 nm, λem = 650–670 nm, (**A1**,**B1**)) and corresponds to the position of mitochondria stained with Mito-Tracker (green channel: λex = 490 nm, λem = 510–516 nm; (**A2**,**B2**)). Colocalization is shown in (**A3**,**B3**) with a merged red and green signal. Electron microscopy (**C**–**F**) demonstrates the ultrastructure of normal fibroblasts (**C**), melanoma cells (**E**) and cells treated with Bis-PMS 5 (**D**,**F**). Exposure of both cell types to 5 µM of Bis-PMS 5 for 2 h induced swelling of mitochondria with cristolysis (**D**,**F**). Asterisks mark mitochondria and arrows mark lipid droplets. Bar is 100 µm (**A**,**B**) and 500 nm (**C**–**F**).

As both Bis-PMSs **5** and **6** rapidly accumulated in the mitochondria in all cell types used in this study, we investigated their possible effect on mitochondrial respiration by employing the Seahorse Bioanalyzer. Parameters reflecting mitochondrial function, such as routine respiration, leak respiration, electron transfer capacity and ATP production, were

measured in melanoma A2058 (Figure 7), glioblastoma U251MG and fibroblast HFP4 cells (Figure S16).

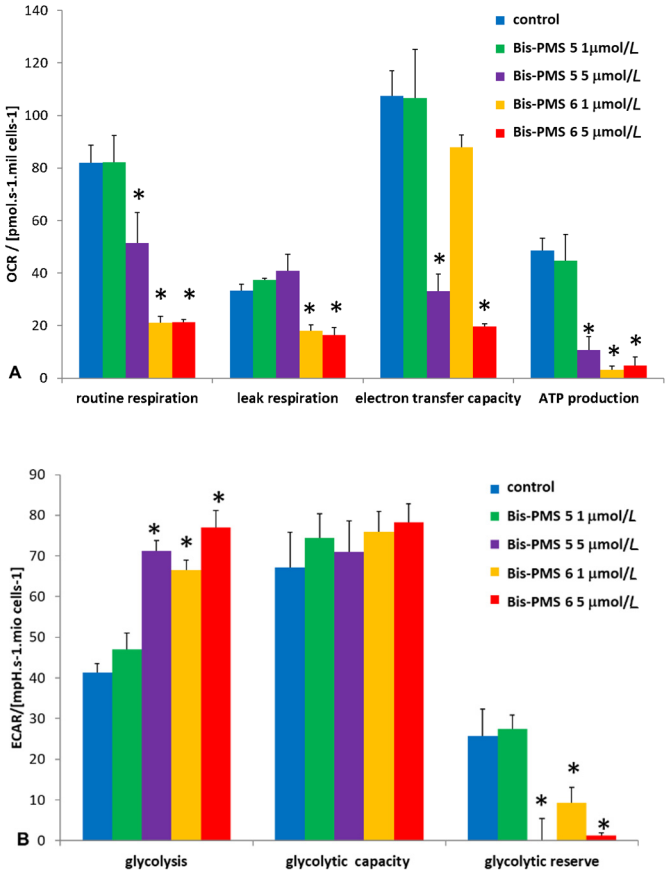


**Figure 7.** Influence of Bis-PMS on the energy metabolism in A2058 melanoma cells. **A** Seahorse Bioanalyzer was used to evaluate mitochondrial respiration (**A**) and glycolysis (**B**) in A2058 cells exposed to 1 and 5 µmol/L of Bis-PMSs **5** and **6** for 2 h. * $p < 0.01$ vs. control, $n = 4$, one-way ANOVA followed by a Tukey's post hoc test. OCR = oxygen consumption rate, ECAR = extracellular acidification rate.

While 1 µM Bis-PMS **5** had no effect on mitochondrial respiration, 5 µM Bis-PMS **5** and both concentrations of Bis-PMS **6** caused a significant reduction in basal and maximal respiration in A2058 cells. These effects were accompanied by enhanced glycolysis as determined by extracellular acidification rate (ECAR) (Figure 7, Figures S17 and S18).

We further evaluated the effect of Bis-PMS on mitochondria using electron microscopy and observed significant changes in mitochondrial morphology in normal fibroblasts, as well as in melanoma cells exposed to Bis-PMS at a concentration inducing metabolic changes (5 µmol/L). The morphological changes were particularly pronounced for Bis-PMS **5** (Figure 6).

After application of Bis-PMSs **5** and **6**, the majority of mitochondria were swollen with only marginal cristae or cristolysis, a clear matrix with a web-like structure and dense aggregates in the lumen (Figures 6, S19 and S20). The mitochondria in control cells without the application of the compounds were without pathological changes and showed typical morphology, a dense matrix and a well-developed system of cristae (Figure S21). Similar morphological changes were induced by Bis-PMSs **5** and **6** in HFP4 fibroblast cells, but they were somewhat smaller than in A2508 melanoma cells (Figures 6, S22 and S23).

Collectively, our results suggest that both Bis-PMSs were cytotoxic for the tested cells, most probably due to their effect on mitochondria, but participation of IL-6R targeting is also possible. Similar results were described for other types of PMSs [27,29,31,32]. Their

cytotoxic effects were also caused by the targeting of mitochondria, as summarized by Leischner Fialova [51]. In the present study, we clearly showed metabolic differences, such as reduced mitochondrial respiration and ensuing increased glycolysis as a compensatory mechanism, in cells treated with Bis-PMSs **5** and **6**. In addition, data published in this study demonstrate that both Bis-PMSs **5** and **6** interact with the receptor for IL-6. IL-6 is produced by cancer-associated fibroblasts and cancer cells and is an important molecule for the exchange of information in the cancer ecosystem [7]. Thus, a dual cytotoxic effect in both Bis-PMSs may be expected.

Does dual targeting make sense? There is a relationship between gp130 and respiration. It has been found that STAT3 participates in the control of cellular respiration in the mitochondria (e.g., complexes I and II of the electron transport chain) [52,53]. In addition, activated STAT3 in the mitochondria can strongly support tumorigenesis [54,55]. In line with this, repression of Il-6-induced STAT3 mitochondrial localization caused increased levels of mitochondrial ROS, collapse of the mitochondrial membrane potential and, subsequently, apoptosis of cancer cells [45].

It should be noted in this context that inhibition of IL-6R and/or gp130 alone can repress cell proliferation, but it is not associated with the activation of apoptotic pathways [3]. Nevertheless, Bis-PMSs **5** and **6** and mono pentamethinium salts also display significant cytotoxicity [28,29]. Due to their fast mitochondrial localization, this effect is most probably associated with alteration of mitochondrial metabolism and/or functionality [29]. Based on these data, the possible mechanism of the anticancer effects of both tested compounds may include inhibition of gp130 signaling, resulting in decreased cell proliferation, and most probably also sensitization of mitochondria to their direct targeting (Figure 8).

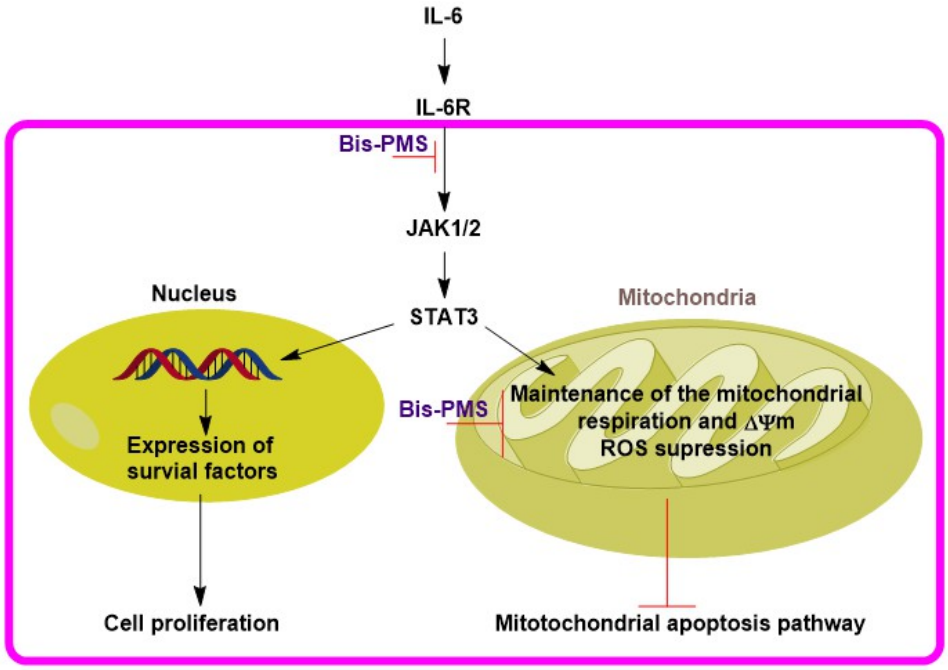


**Figure 8.** Proposed anticancer mechanism for Bis-PMSs **5** and **6**. Decreased activity of IL-6R via IL-6Rβ (gp130) targeting may cause lower levels of activated/phosphorylated STAT3. The decrease in STAT3 activity reduces expression of survival factors and mitochondrial functionality. As a result, cell proliferation is repressed and the mitochondrial apoptotic pathway is activated, respectively. Simultaneously, direct inhibition of mitochondrial metabolism by Bis-PMSs **5** and **6** leads to decreased cell growth and cell death.

This dual alteration of mitochondrial metabolism (inhibition of gp130 and direct mitochondrial targeting) could be an effective method for inducing apoptosis in cancer

cells with activated IL-6 signaling. However, other studies are needed to optimize, or reject, this novel therapeutic strategy.

Our results suggest that the structural motif of bis-pentamethinium salts could be applied in the design of novel anticancer drugs for the combined targeting of IL-6R and mitochondrial respiration. There are nevertheless several challenging aspects.

Firstly, simultaneous inhibition of mitochondrial respiration and IL-6R can be complicated by the different subcellular localization of the targets. IL-6R is localized on the cell surface, while targeting mitochondrial respiration requires efficient mitochondrial uptake. Pentamethinium salts with aromatic substitution in the γ-position usually display rapid mitochondrial localization due to strong affinity for cardiolipin [28,29]. For example, mitochondrial localization of indolium pentamethine can be observed after 5–10 min [28]. In the case of Bis-PMSs **5** and **6**, mitochondrial uptake was not that fast. This intracellular accumulation may nevertheless limit the availability of the compounds to inhibit IL-6R. On the other hand, pentamethinium with aromatic substitution in the γ-position could represent a promising structure motif for the targeting of pathological mitochondria, such as those with lower mitochondrial potential [28,29]. It is well-known that cancer cells can display significantly decreased mitochondrial membrane potential compared to healthy cells [56].

Secondly, although gp130 (IL-6Rβ) is an essential part of the IL-6R and its inhibition blocks signal transduction, it also participates in the signaling of other members of the IL-6/IL-12 family (e.g., IL-11, IL-23 and IL-35) [57]. The binding of both bis-pentamethinium salts to gp130 thus implies they not only block IL-6 signaling. However, in terms of their possible therapeutic application, this may be beneficial. For example, IL-11 activates IL-11RA and gp130/STAT3 signaling and plays an important role in tumorigenesis. Its higher levels can stimulate tumor immune evasion and metastatic spread and are associated with disease progression and poor patient outcome [58].

Thirdly, although both Bis-PMSs **5** and **6** decreased secretion of alkaline phosphatase controlled by STAT3 in the HEK reported cells, the inhibitory effect was substantially lower compared to tocilizumab (Figure S9). Furthermore, we cannot exclude the possibility that the decreased alkaline phosphatase secretion could have been partially caused by the effect of the compounds on mitochondria.

Fourthly, selectivity for cancer cells remains an important issue. Although bis-PMSs **5** and **6** represent promising compounds, they also inhibit growth and metabolic activity in non-malignant cells. Further studies are needed to identify derivatives with selective accumulation in the tumor tissue and/or more selective effects on cancer cells.

## 4. Conclusions

New-generation heterocyclic bis-pentamethinium salts **5** and **6** were prepared from phenylenediacetic acids, which were converted into corresponding bis-vinamidinium intermediates (**1, 2**) and, subsequently, to bis-malondialdehydes (**3**, **4**). The reaction of quaternary indolium salt with bis-vinamidinium salts (**1**, **2**) or with bis-malondialdehydes (**3**, **4**) produced target the Bis-PMSs (**5**, **6**) in low and moderate yields, respectively.

Docking studies and microscale thermophoresis assays showed that both bis-pentamethinium salts **5** and **6** displayed high affinity for IL-6R. In addition, both compounds rapidly accumulated in mitochondria, repressed mitochondrial respiration with compensatory enhancement of glycolysis and altered mitochondrial morphology. These effects are most likely responsible for the cytotoxicity of the compounds towards a wide spectrum of cancer cells. The new Bis-PMSs thus represent a promising structure motif for multitargeting compounds interfering with IL-6 signaling and simultaneously impacting mitochondria, an emerging target for anticancer therapy [59]. Future studies modifying their structure to increase the selectivity for cancer cells are warranted.

**Supplementary Materials:** The following supporting information can be downloaded at: https://www.mdpi.com/article/10.3390/pharmaceutics14081712/s1, Figure S1: Absorption spectra of Bis-PMSs **5** and **6** in four different solvents, Figure S2: Excitation and emission spectra of Bis-PMS **5** in four different solvents, Figure S3: Excitation and emission spectra of Bis-PMS **6** in four different solvents, Figure S3: Normalized bleaching curves of Bis-PMSs **5** and **6**, Figure S4: Absorption spectra of Bis-PMS **5** after incubation points in EMEM with and without MeOH, Figure S5: Absorption spectra of Bis-PMS **6** after incubation points in EMEM with and without MeOH, Figure S6: Normalized bleaching curves of Bis-PMSs **5** and **6,** Figure S7: Interaction of mono pentamethinium salts with a 3D model of IL-6R, Figure S8: Interaction of mono pentamethinium salts with the residues of the homology model of IL-6R, Figure S9: Effect of bis-pentamethinium salts **5** and **6** on the IL-6 signaling cascade, Figure S10: Cytotoxity of Bis-PMS **5**, Figure S11: Cytotoxity of Bis-PMS **6**, Figure S12: Cytotoxity of Bis-PMSs **5** and **6**, Figure S13: In vitro localization of Bis-PMS **5**, Figure S14: In vitro localization of Bis-PMS **6,** Figure S15: Two-dimensional (2D) scatter plots of fluorescent probes for Bis-PMSs **5** and **6** versus MitoTracker, Figure S16: Influence of Bis-PMSs **5** and **6** on mitochondrial metabolism and respiration, Figure S17: Influence of Bis-PMSs **5** and **6** on glycolytic function, Figure S18: Measurements of respiration (OCR) and glycolysis (ECAR) of melanoma cells, Figure S19: Influence of Bis-PMS **5** on mitochondrial morphology of A2058 cells. Figure S20: Influence of Bis-PMS **6** on mitochondrial morphology of A2058 cells, Figure S21: Mitochondrial morphology of HFP4, Figure S22: Influence of Bis-PMS **5** on mitochondrial morphology of HFP4 cells, Figure S23: Influence of Bis-PMS **6** on mitochondrial morphology of HFP4 cells; Table S1: Excitation and emission maxima of Bis-pentamethinium salts **5** and **6**, Table S2: Interaction mode of Bis-pentamethinium salts **5** and **6** with amino acid residue of IL-6R, Table S3: Cytotoxicity of Bis-PMSs **5** and **6** in normal and cancer cells.

**Author Contributions:** Investigation, V.T., Z.K., R.K., K.V., N.A., L.L., K.S., B.D., L.Z., E.V., P.B. and M.H.M.; Conceptualization, P.M., M.M., P.B., J.K., H.H., V.F., A.Š. and K.S.J., Writing and Original Draft Preparation, K.S.J. and M.J.; Writing, M.J.; Editing, L.L., K.S.J., P.B., A.Š. and M.J.; Funding acquisition, K.S.J. All authors have read and agreed to the published version of the manuscript.

**Funding:** This work was supported by the projects of Charles University in Prague (SVV260521; UNCE 204064). This work was supported by the Cooperatio Program. This work was also supported by the Ministry of Education, Youth and Sports, grant no. LM2018133 (EATRIS-CZ). The research was also funded by the Technology Agency of the Czech Republic within the projects with nos. TN01000013 and FW02020128 and by the Ministry of Health of the Czech Republic (grant nos. NU21-08-00407 and NU22-D-136). We also acknowledge the Operational Program "Research, Development and Education" within the project: Center for Tumor Ecology—Research of the Cancer Microenvironment Supporting Cancer Growth and Spread (reg. no. CZ.02.1.01/0.0/0.0/16_019/0000785). Other support was from the projects Excelles, ID Project no. LX22NPO5102, funded by the European Union—Next Generation EU, MH CZ-DRO—VFN64165 and SVV—UK26037.

**Institutional Review Board Statement:** Not applicable.

**Informed Consent Statement:** Not applicable.

**Data Availability Statement:** Not applicable.

**Acknowledgments:** The authors are grateful to Šárka Takáčová for excellent revision of English in the manuscript. We would also like to thank Tomáš Bříza, who played an irreplaceable role in the design and synthesis of many polymethnium salts, including Bis-PMSs **5** and **6**. We honor his memory. We acknowledge the Electron Microscopy Core Facility, IMG CAS, Prague, Czech Republic, supported by MEYS CR (LM2018129 Czech-BioImaging) and ERDF (projects: Z.02.1.01/0.0/0.0/18_046/0016045, CZ.02.1.01/0.0/0.0/16_013/0001775), for their support in obtaining the scientific data presented in this paper.

**Conflicts of Interest:** The authors declare no conflict of interest.

## References

1. Hirano, T.; Akira, S.; Taga, T.; Kishimoto, T. Biological and clinical aspects of interleukin 6. *Immunol. Today* **1990**, *11*, 443–449. [CrossRef]
2. Chonov, D.C.; Ignatova, M.M.K.; Ananiev, J.R.; Gulubova, M.V. IL-6 Activities in the Tumour Microenvironment. Part 1. *Open Access Maced. J. Med Sci.* **2019**, *7*, 2391–2398. [CrossRef]

3. Brábek, J.; Jakubek, M.; Vellieux, F.; Novotný, J.; Kolář, M.; Lacina, L.; Szabo, P.; Strnadová, K.; Rösel, D.; Dvořánková, B.; et al. Interleukin-6: Molecule in the Intersection of Cancer, Ageing and COVID-19. *Int. J. Mol. Sci.* **2020**, *21*, 7937. [CrossRef] [PubMed]
4. Hill, D.G.; Ward, A.; Nicholson, L.B.; Jones, G.W. Emerging roles for IL-6 family cytokines as positive and negative regulators of ectopic lymphoid structures. *Cytokine* **2021**, *146*, 155650. [CrossRef] [PubMed]
5. Slominski, R.M.; Tuckey, R.; Manna, P.R.; Jetten, A.M.; Postlethwaite, A.; Raman, C.; Slominski, A.T. Extra-adrenal glucocorticoid biosynthesis: Implications for autoimmune and inflammatory disorders. *Genes Immun.* **2020**, *21*, 150–168. [CrossRef]
6. Mouawad, R.; Benhammouda, A.; Rixe, O.; Antoine, E.C.; Borel, C.; Weil, M.; Khayat, D.; Soubrane, C. Endogenous interleukin 6 levels in patients with metastatic malignant melanoma: Correlation with tumor burden. *Clin. Cancer Res.* **1996**, *2*, 1405–1409.
7. Španko, M.; Strnadová, K.; Pavlíček, A.J.; Szabo, P.; Kodet, O.; Valach, J.; Dvořánková, B.; Smetana, K., Jr.; Lacina, L. IL-6 in the Ecosystem of Head and Neck Cancer: Possible Therapeutic Perspectives. *Int. J. Mol. Sci.* **2021**, *22*, 11027. [CrossRef]
8. Johnson, D.E.; O'Keefe, R.A.; Grandis, J.R. Targeting the IL-6/JAK/STAT3 signalling axis in cancer. *Nat. Rev. Clin. Oncol.* **2018**, *15*, 234–248. [CrossRef]
9. Hoejberg, L.; Bastholt, L.; Johansen, J.S.; Christensen, I.J.; Gehl, J.; Schmidt, H. Serum interleukin-6 as a prognostic biomarker in patients with metastatic melanoma. *Melanoma Res.* **2012**, *22*, 287–293. [CrossRef]
10. Kumari, N.; Dwarakanath, B.S.; Das, A.; Bhatt, A.N. Role of interleukin-6 in cancer progression and therapeutic resistance. *Tumor Biol.* **2016**, *37*, 11553–11572. [CrossRef]
11. Gu, J.; Wang, J.; Liu, X.; Sai, K.; Mai, J.; Xing, F.; Chen, Z.; Yang, X.; Lu, W.; Guo, C.; et al. IL-6 derived from therapy-induced senescence facilitates the glycolytic phenotype in glioblastoma cells. *Am. J. Cancer Res.* **2021**, *11*, 458–478. [PubMed]
12. Kadauke, S.; Myers, R.M.; Li, Y.; Aplenc, R.; Baniewicz, D.; Barrett, D.M.; Leahy, A.B.; Callahan, C.; Dolan, J.G.; Fitzgerald, J.C.; et al. Risk-Adapted Preemptive Tocilizumab to Prevent Severe Cytokine Release Syndrome After CTL019 for Pediatric B-Cell Acute Lymphoblastic Leukemia: A Prospective Clinical Trial. *J. Clin. Oncol.* **2021**, *39*, 920–930. [CrossRef] [PubMed]
13. Hagi, T.; Nakamura, T.; Kita, K.; Iino, T.; Asanuma, K.; Sudo, A. Anti-tumour effect of tocilizumab for osteosarcoma cell lines. *Bone Jt. Res.* **2020**, *9*, 821–826. [CrossRef] [PubMed]
14. Shiroshita, K.; Kikuchi, T.; Okayama, M.; Kasahara, H.; Kamiya, T.; Shimizu, T.; Kurose, N.; Masaki, Y.; Okamoto, S. Interleukin-6-producing Intravascular Large B-cell Lymphoma with Lymphadenopathy Mimicking the Histology of Multicentric Castleman Disease. *Intern. Med.* **2020**, *59*, 3061–3065. [CrossRef]
15. Mintz, C.S.; Crea, R. Protein scaffolds: The next generation of protein therapeutics? *Bioprocess Int.* **2013**, *11*, 40–48, 51.
16. Aqel, S.I.; Kraus, E.E.; Jena, N.; Kumari, V.; Granitto, M.C.; Mao, L.; Farinas, M.F.; Zhao, E.Y.; Perottino, G.; Pei, W.; et al. Novel small molecule IL-6 inhibitor suppresses autoreactive Th17 development and promotes Treg development. *Clin. Exp. Immunol.* **2019**, *196*, 215–225. [CrossRef]
17. Enomoto, A.; Rho, M.C.; Fukami, A.; Hiraku, O.; Komiyama, K.; Hayashi, M. Suppression of cancer cachexia by 20*S*,21-epoxy-resibufogenin-3-acetate—A novel nonpeptide IL-6 receptor antagonist. *Biochem. Biophys. Res. Commun.* **2004**, *323*, 1096–1102. [CrossRef]
18. Enomoto, A.; Rho, M.C.; Komiyama, K.; Hayashi, M. Inhibitory Effects of Bufadienolides on Interleukin-6 in MH-60 Cells. *J. Nat. Prod.* **2004**, *67*, 2070–2072. [CrossRef]
19. Hayashi, M.; Kim, Y.P.; Takamatsu, S.; Enomoto, A.; Shinose, M.; Takahashi, Y.; Tanaka, H.; Komiyama, K.; Omura, S. Madindoline, a Novel Inhibitor of IL-6 Activity from *Streptomyces* sp. K93-0711. I. Taxonomy, Fermentation, Isolation and Biological Activities. *J. Antibiot.* **1996**, *49*, 1091–1095. [CrossRef]
20. Hayashi, M.; Rho, M.C.; Enomoto, A.; Fukami, A.; Kim, Y.P.; Kikuchi, Y.; Sunazuka, T.; Hirose, T.; Komiyama, K.; Omura, S. Suppression of bone resorption by madindoline A, a novel nonpeptide antagonist to gp130. *Proc. Natl. Acad. Sci. USA* **2002**, *99*, 14728–14733. [CrossRef]
21. Hayashi, M.; Rho, M.C.; Fukami, A.; Enomoto, A.; Nonaka, S.; Sekiguchi, Y.; Yanagisawa, T.; Yamashita, A.; Nogawa, T.; Kamano, Y.; et al. Biological Activity of a Novel Nonpeptide Antagonist to the Interleukin-6 Receptor 20*S*,21-Epoxy-resibufogenin-3-formate. *J. Pharmacol. Exp. Ther.* **2002**, *303*, 104–109. [CrossRef]
22. Hong, S.S.; Choi, J.H.; Lee, S.Y.; Park, Y.H.; Park, K.Y.; Lee, J.Y.; Kim, J.; Gajulapati, V.; Goo, J.I.; Singh, S.; et al. A Novel Small-Molecule Inhibitor Targeting the IL-6 Receptor β Subunit, Glycoprotein 130. *J. Immunol.* **2015**, *195*, 237–245. [CrossRef] [PubMed]
23. Kino, T.; Boos, T.L.; Sulima, A.; Siegel, E.M.; Gold, P.W.; Rice, K.C.; Chrousos, G.P. 3-O-Formyl-20R,21-epoxyresibufogenin suppresses IL-6–type cytokine actions by targeting the glycoprotein 130 subunit: Potential clinical implications. *J. Allergy Clin. Immunol.* **2007**, *120*, 437–444. [CrossRef] [PubMed]
24. Saleh, A.Z.M.; Greenman, K.L.; Billings, S.; Van Vranken, D.L.; Krolewski, J.J. Binding of Madindoline A to the Extracellular Domain of gp130. *Biochemistry* **2005**, *44*, 10822–10827. [CrossRef]
25. Wang, J.; Qiao, C.; Xiao, H.; Lin, Z.; Li, Y.; Zhang, J.; Shen, B.; Fu, T.; Feng, J. Structure-based virtual screening and characterization of a novel IL-6 antagonistic compound from synthetic compound database. *Drug Des. Dev. Ther.* **2016**, *10*, 4091–4100. [CrossRef]
26. Yamamoto, D.; Sunazuka, T.; Hirose, T.; Kojima, N.; Kaji, E.; Omura, S. Design, synthesis, and biological activities of madindoline analogues. *Bioorganic Med. Chem. Lett.* **2006**, *16*, 2807–2811. [CrossRef]
27. Bříza, T.; Králová, J.; Dolenský, B.; Rimpelová, S.; Kejík, Z.; Ruml, T.; Hajdúch, M.; Džubák, P.; Mikula, I.; Martásek, P.; et al. Striking Antitumor Activity of a Methinium System with Incorporated Quinoxaline Unit Obtained by Spontaneous Cyclization. *ChemBioChem A Eur. J. Chem. Biol.* **2015**, *16*, 555–558. [CrossRef]

28. Bříza, T.; Rimpelová, S.; Králová, J.; Záruba, K.; Kejík, Z.; Ruml, T.; Martásek, P.; Král, V. Pentamethinium fluorescent probes: The impact of molecular structure on photophysical properties and subcellular localization. *Dye. Pigment.* **2014**, *107*, 51–59. [CrossRef]
29. Rimpelová, S.; Bříza, T.; Králová, J.; Záruba, K.; Kejík, Z.; Císařová, I.; Martásek, P.; Ruml, T.; Král, V. Rational Design of Chemical Ligands for Selective Mitochondrial Targeting. *Bioconjugate Chem.* **2013**, *24*, 1445–1454. [CrossRef]
30. Krejcir, R.; Krcova, L.; Zatloukalova, P.; Briza, T.; Coates, P.J.; Sterba, M.; Muller, P.; Kralova, J.; Martasek, P.; Kral, V.; et al. A Cyclic Pentamethinium Salt Induces Cancer Cell Cytotoxicity through Mitochondrial Disintegration and Metabolic Collapse. *Int. J. Mol. Sci.* **2019**, *20*, 4208. [CrossRef]
31. Bříza, T.; Králová, J.; Rimpelová, S.; Havlík, M.; Kaplánek, R.; Kejík, Z.; Martásek, P.; Mikula, I.; Džubák, P.; Hajdúch, M.; et al. Pentamethinium salts as ligands for cancer: Sulfated polysaccharide co-receptors as possible therapeutic target. *Bioorganic Chem.* **2018**, *82*, 74–85. [CrossRef] [PubMed]
32. Krejcir, R.; Briza, T.; Sterba, M.; Simoncik, O.; Muller, P.; Coates, P.J.; Martasek, P.; Vojtesek, B.; Zatloukalova, P. Anticancer pentamethinium salt is a potent photosensitizer inducing mitochondrial disintegration and apoptosis upon red light illumination. *J. Photochem. Photobiol. B Biol.* **2020**, *209*, 111939. [CrossRef] [PubMed]
33. Sestito, S.; Runfola, M.; Tonelli, M.; Chiellini, G.; Rapposelli, S. New Multitarget Approaches in the War against Glioblastoma: A Mini-Perspective. *Front. Pharmacol.* **2018**, *9*, 874. [CrossRef] [PubMed]
34. Habashi, F.; Mehranpour, A.; Jahromi, E.B. Synthesis and characterization of new derivatives of bis(1,4-diazepinium) salts and bis(γ-substituted pentamethine cyanine(dyes using vinamidinium salt. *J. Heterocycl. Chem.* **2020**, *57*, 2428–2432. [CrossRef]
35. Choi, H.J.; Dincă, M.; Long, J.R. Broadly Hysteretic $H_2$ Adsorption in the Microporous Metal−Organic Framework Co(1,4-benzenedipyrazolate). *J. Am. Chem. Soc.* **2008**, *130*, 7848–7850. [CrossRef]
36. Lozan, V.; Solntsev, P.Y.; Leibeling, G.; Domasevitch, K.V.; Kersting, B. Tetranuclear Nickel Complexes Composed of Pairs of Dinuclear LNi 2 Fragments Linked by 4,4′-Bipyrazolyl, 1,4-Bis(4′-pyrazolyl)benzene, and 4,4′-Bipyridazine: Synthesis, Structures, and Magnetic Properties. *Eur. J. Inorg. Chem.* **2007**, *2007*, 3217–3226. [CrossRef]
37. Church, R.; Trust, R.; Albright, J.D.; Powell, D. New Synthetic Routes to 3-, 5-, and 6-Aryl-2-chloropyridines. *J. Org. Chem.* **1995**, *60*, 3750–3758. [CrossRef]
38. Liu, Y.; Grimm, M.; Dai, W.T.; Hou, M.C.; Xiao, Z.X.; Cao, Y. CB-Dock: A web server for cavity detection-guided protein–ligand blind docking. *Acta Pharmacol. Sin.* **2020**, *41*, 138–144. [CrossRef]
39. *BIOVIA Discovery Studio Modeling Environment*; Dassault Systèmes BIOVIA: San Diego, CA, USA, 2017.
40. Busek, P.; Stremenova, J.; Sromova, L.; Hilser, M.; Balaziova, E.; Kosek, D.; Trylcova, J.; Strnad, H.; Krepela, E.; Sedo, A. Dipeptidyl peptidase-IV inhibits glioma cell growth independent of its enzymatic activity. *Int. J. Biochem. Cell Biol.* **2012**, *44*, 738–747. [CrossRef]
41. Zdrazilova, L.; Hansikova, H.; Gnaiger, E. Comparable respiratory activity in attached and suspended human fibroblasts. *PLoS ONE* **2022**, *17*, e0264496. [CrossRef]
42. Mehranpour, A.M.; Hashemnia, S.; Maghamifar, R. Synthesis and Characterization of New γ-Substituted Pentamethine Cyanine Dyes. *Synth. Commun.* **2010**, *40*, 3594–3602. [CrossRef]
43. Matichak, J.D.; Hales, J.M.; Barlow, S.; Perry, J.W.; Marder, S.R. Dioxaborine- and Indole-Terminated Polymethines: Effects of Bridge Substitution on Absorption Spectra and Third-Order Polarizabilities. *J. Phys. Chem. A* **2011**, *115*, 2160–2168. [CrossRef] [PubMed]
44. Mehranpour, A.M.; Hashemnia, S.; Azamifar, F. Synthesis and Characterization of γ-Heteroaryl-substituted Pentamethine Cyanine Dyes with Carboxy or Methoxycarbonyl Substituents at the Two Heterocyclic End Groups. *J. Heterocycl. Chem.* **2014**, *51*, 1457–1462. [CrossRef]
45. MacKenzie, G.G.; Huang, L.; Alston, N.; Ouyang, N.; Vrankova, K.; Mattheolabakis, G.; Constantinides, P.P.; Rigas, B. Targeting Mitochondrial STAT3 with the Novel Phospho-Valproic Acid (MDC-1112) Inhibits Pancreatic Cancer Growth in Mice. *PLoS ONE* **2013**, *8*, e61532. [CrossRef]
46. Bříza, T.; Kejík, Z.; Císařová, I.; Králová, J.; Martásek, P.; Král, V. Optical sensing of sulfate by polymethinium salt receptors: Colorimetric sensor for heparin. *Chem. Commun.* **2008**, *16*, 1901–1903. [CrossRef]
47. Kejík, Z.; Bříza, T.; Králová, J.; Mikula, I.; Poučková, P.; Martásek, P.; Král, V. New method for recognition of sterol signalling molecules: Methinium salts as receptors for sulphated steroids. *Steroids* **2015**, *94*, 15–20. [CrossRef]
48. Abeywardena, M.; Leifert, W.; Warnes, K.; Varghese, J.; Head, R. Cardiovascular Biology of Interleukin-6. *Curr. Pharm. Des.* **2009**, *15*, 1809–1821. [CrossRef]
49. Mihara, M.; Kasutani, K.; Okazaki, M.; Nakamura, A.; Kawai, S.; Sugimoto, M.; Matsumoto, Y.; Ohsugi, Y. Tocilizumab inhibits signal transduction mediated by both mIL-6R and sIL-6R, but not by the receptors of other members of IL-6 cytokine family. *Int. Immunopharmacol.* **2005**, *5*, 1731–1740. [CrossRef]
50. Yang, J.; Qian, S.; Cai, X.; Lu, W.; Hu, C.; Sun, X.; Yang, Y.; Yu, Q.; Gao, S.P.; Cao, P. Chikusetsusaponin IVa Butyl Ester (CS-IVa-Be), a Novel IL6R Antagonist, Inhibits IL6/STAT3 Signaling Pathway and Induces Cancer Cell Apoptosis. *Mol. Cancer Ther.* **2016**, *15*, 1190–1200. [CrossRef]
51. Fialova, J.L.; Raudenska, M.; Jakubek, M.; Kejik, Z.; Martasek, P.; Babula, P.; Matkowski, A.; Filipensky, P.; Masarik, M. Novel Mitochondria-targeted Drugs for Cancer Therapy. *Mini-Rev. Med. Chem.* **2021**, *21*, 816–832. [CrossRef]
52. Wegrzyn, J.; Potla, R.; Chwae, Y.J.; Sepuri, N.B.V.; Zhang, Q.; Koeck, T.; Derecka, M.; Szczepanek, K.; Szelag, M.; Gornicka, A.; et al. Function of Mitochondrial Stat3 in Cellular Respiration. *Science* **2009**, *323*, 793–797. [CrossRef] [PubMed]

53. Mantel, C.; Messina-Graham, S.; Moh, A.; Cooper, S.; Hangoc, G.; Fu, X.Y.; Broxmeyer, H.E. Mouse hematopoietic cell–targeted STAT3 deletion: Stem/progenitor cell defects, mitochondrial dysfunction, ROS overproduction, and a rapid aging–like phenotype. *Blood* **2012**, *120*, 2589–2599. [CrossRef] [PubMed]
54. Gough, D.J.; Corlett, A.; Schlessinger, K.; Wegrzyn, J.; Larner, A.C.; Levy, D.E. Mitochondrial STAT3 Supports Ras-Dependent Oncogenic Transformation. *Science* **2009**, *324*, 1713–1716. [CrossRef] [PubMed]
55. Zhang, Q.; Raje, V.; Yakovlev, V.; Yacoub, A.; Szczepanek, K.; Meier, J.; Derecka, M.; Chen, Q.; Hu, Y.; Sisler, J.; et al. Mitochondrial Localized Stat3 Promotes Breast Cancer Growth via Phosphorylation of Serine 727. *J. Biol. Chem.* **2013**, *288*, 31280–31288. [CrossRef]
56. Tomita, K.; Kuwahara, Y.; Igarashi, K.; Roudkenar, M.H.; Roushandeh, A.M.; Kurimasa, A.; Sato, T. Mitochondrial Dysfunction in Diseases, Longevity, and Treatment Resistance: Tuning Mitochondria Function as a Therapeutic Strategy. *Genes* **2021**, *12*, 1348. [CrossRef]
57. Scheller, J.; Berg, A.; Moll, J.M.; Floss, D.M.; Jungesblut, C. Current status and relevance of single nucleotide polymorphisms in IL-6-/IL-12-type cytokine receptors. *Cytokine* **2021**, *148*, 155550. [CrossRef]
58. To, S.Q.; Dmello, R.S.; Richards, A.K.; Ernst, M.; Chand, A.L. STAT3 Signaling in Breast Cancer: Multicellular Actions and Therapeutic Potential. *Cancers* **2022**, *14*, 429. [CrossRef]
59. Vasan, K.; Werner, M.; Chandel, N.S. Mitochondrial Metabolism as a Target for Cancer Therapy. *Cell Metab.* **2020**, *32*, 341–352. [CrossRef]